Shape- and Size-Controlled Synthesis of Monoclinic ErOOH and Cubic Er_2O_3 from Micro- to Nanostructures and Their Upconversion Luminescence

Thanh-Dinh Nguyen, Cao-Thang Dinh, and Trong-On Do*

Department of Chemical Engineering, Laval University, Quebec G1K 7P4, Canada

ABSTRACT A general approach has been developed for the synthesis of monoclinic ErOOH and cubic Er_2O_3 structures with high yield and controlled size and shape *via* the solvo-hydrothermal reaction of erbium nitrate in water/ethanol/decanoic acid media. The monoclinic ErOOH phase was formed at relatively low temperature (120—140 °C); however, the cubic Er_2O_3 phase was obtained at higher temperature (160—180 °C). By simply tuning different experimental parameters, such as the reaction temperature, the concentration of decanoic acid and erbium precursor *etc.*, different sizes from 3 nm to 3 μm, and a variety of shapes including cores/dots to spheres, wrinkle-surfaced spheres, flowers, dog bonds, wires, rods, bundles, straw sheaves, and brooms can be achieved. The particle size of products decreased from micro- to nanometer as the decanoic acid concentration increased from 0.038 to 0.190 M. Furthermore, by using anhydrous ethanol instead of water—ethanol solvents, the particle size significantly decreased from 18 nm spheres to 3 nm cores. At high precursor monomer concentrations (76.25—152.50 mM), the nanorods were also obtained due to the anisotropic growth. On the basis of this study, a correlation between the experimental parameters and the phase, shape, and size of the products was proposed. The upconversion luminescence properties depend not only on crystalline phase but also on particle size of the products. The luminescence intensity increases with the decrease of particle size from micro- to nanometers.

KEYWORDS: shape-controlled · erbium compound micro/nanostructures · spheres · flowers · straw sheaves · bundles · rods

The shape, size, and phase of materials with dependent properties are well-established. The synthesis of metal oxide particles with controllable shape, size, and phase is thus a key goal in materials chemistry.[1,2] Specific morphologies such as nanorods, nanowires, nanocores, nanodots, nanobundles, nanospheres, and nanoflowers show great promise in many applications, as they usually exhibit electronic, optical, magnetic, and catalytic properties which are distinct as compared to their corresponding bulk materials.[3−5] In addition, the specific properties of three-dimensional architecture assemblies can be found as a result of the mutual order interparticle arrangement.[6,7] To achieve precise size/shape control, it is important to understand the relationship between product morphologies and experimental parameters. In the colloidal synthesis, the choice of appropriate surfactants and the synthetic conditions are crucial for controlling nucleation and growth in manipulating the size, shape, and phase of the resulting nanostructures.[8−12] The formation of nanocrystals can be based on Ostwald ripening,[13] in which the growth of larger crystals occurs at the expense of smaller crystals. Nanoparticles can undergo self-assembly to 2D and 3D superstructures by oriented attachment[14] and lateral aggregation.[15] These mechanism features can be thus important clues to the microstructural formation from primary building unit assembly.

Erbium compound (ErOOH and Er_2O_3) materials are recognized as one of the most important rare earth oxides for sensing applications in the lasers and optical amplifiers.[16−18] Indeed, the unique properties of these materials are produced by the intra Er^{3+} 4f shell transition from its first excited state ($^4I_{3/2}$) to the ground state ($^4I_{5/2}$). This is related to the emission band of around 1.54 μm that is one of the standard telecommunication wavelengths.[19,20] Previous investigations indicate that the intrinsic minimum optical absorption of erbium compound materials strongly depends on shape and size and crystalline phase.[21−24] A recent study is directed to erbium compounds due to their special capability of near-infrared excitation (NIR)-to-visible upconversion (UC) emission.[25] Developing new and simple methods for shape-, size-, and phase-controlled synthesis of ErOOH and Er_2O_3 materials on the micro/nanoscales would thus open up new avenues for uncovering their remarkable properties and

*Address correspondence to trong-on.do@gch.ulaval.ca.

Received for review December 5, 2009 and accepted March 26, 2010.

Published online April 7, 2010.
10.1021/nn100292s

TABLE 1. Synthesis Conditions, Crystal Phases, and Morphologies of Monoclinic ErOOH and Cubic Er_2O_3 Micro- and Nanostructures[a]

sample	precursor (mM)	ethanol (mL)	water (mL)	decanoic acid (M)	temperature (°C)	product	structure	shape	size (nm)
1	7.63, Er^{3+}	30	10	0.038	120	ErOOH	monoclinic	quasi-sphere	3000
2	7.63, Er^{3+}	30	10	0.038	140	ErOOH	monoclinic	aggregated-sphere	3000
3	7.63, Er^{3+}	30	10	0.038	160	Er_2O_3	cubic	wrinkle-sphere	3000
4	7.63, Er^{3+}	30	10	0.038	180	Er_2O_3	cubic	flower	3000
5	7.63, Er^{3+}	30	10	0.152	120	ErOOH	monoclinic	wire-bundle	100 × 400
6	7.63, Er^{3+}	30	10	0.152	140	ErOOH	monoclinic	straw-sheaf	150 × 700
7	7.63, Er^{3+}	30	10	0.152	160	Er_2O_3	cubic	broom	150 × 350
8	7.63, Er^{3+}	30	10	0.076	180	Er_2O_3	cubic	flower	3000
9	7.63, Er^{3+}	30	10	0.114	180	Er_2O_3	cubic	dog-bond	18
10	7.63, Er^{3+}	30	10	0.152	180	Er_2O_3	cubic	sphere	18
11	7.63, Er^{3+}	30	10	0.190	180	Er_2O_3	cubic	dot	3
12	7.63, Er^{3+}	40	0	0.152	180	Er_2O_3	cubic	core	3
13	7.63, $Er(OH)_3$	30	10	0.152	180	Er_2O_3	cubic	dot	4
14	76.25, $Er(OH)_3$	30	10	0.152	180	Er_2O_3	cubic	wire	80 × 150
15	152.50, $Er(OH)_3$	30	10	0.152	180	Er_2O_3	cubic	rod	250 × 1000

[a]All samples were synthesized by hydro-solvothermal process for 24 h.

for achieving useful applications in optical telecommunication. Furthermore, due to their size-, shape-, and phase-dependent properties, direct syntheses of tridimensional (3D) structures using surfactants have been extensively studied. However, little work has been reported concerning 3D erbium compound materials with controllable size, from micro- to nanostructures, and shapes such as spheres, wrinkle-surfaced spheres, and flowers. For example, Gao and co-workers[26] synthesized 200−300 nm sized erbium oxide microspheres using urea as the precipitant of erbium ion precursors without any surfactants under hydrothermal condition. Li *et al.*[27] reported a hydrothermal route for the synthesis of erbium hydroxide nanobelts from the metal hydroxide precursors. However, it is hard to control the size and shape of the products, due to the absence of capping agents. In a recent study, we reported a two-phase (toluene−water) method for synthesis of uniform Er_2O_3 nanospheres *via* the decomposition of erbium−oleate complex precursors in the presence of capping oleylamine/*tert*-butylamine ligands.[28] It was illustrated that a nucleophilic reaction is required between $Er(oleate)_3$ and *tert*-butylamine, *via* an S_N1 mechanism, to generate erbium monomers[29] and subsequent growth of oleylamine-capped erbium oxide nuclei at the water−toluene interface; this step is followed by particle growth. The products are hydrophobic and highly dispersed in the toluene phase (nonpolar solution), and no product was observed in the water phase. This method leads exclusively to cubic-phase Er_2O_3 nanocrystals; however, at relatively high temperature (≥180 °C) due to the highly thermal stability of the erbium−oleate complex.[30,31] Because Er_2O_3 nanocrystals are a technologically important material and have widespread applications in various areas of research, the development of a new and simple method at low temperature for the synthesis of these nanocrystals with controlled size and shape is of particular interest.

In this paper, we report a new and straightforward approach toward the shape-, size-, and phase- controlled synthesis of ErOOH and Er_2O_3 micro- and nanostructures in high yield, using erbium nitrate precursors and the capping molecule, decanoic acid. The reactions take place in a water/ethanol solution, a "one polar phase" system at the relatively low temperature of ≤180 °C. The capping products were precipitated at the bottom of a Teflon cup instead of becoming dispersed in the toluene phase as described in previous two-phase methods. This synthetic procedure offers several advantages such as the use of nontoxic and inexpensive reagents and mild reaction conditions with phase, size, and shape control. By only tuning the temperature in the reaction system, monoclinic ErOOH and cubic Er_2O_3 phases can be obtained. Furthermore, various particle sizes in the range of thousands to tens of nanometers and a variety of shapes can be achieved simply by varying the synthetic conditions including the concentration of decanoic acid and erbium precursor and the amount of water. The crystalline phase- and particle size-dependent optical properties of these micro/nanomaterials are also discussed.

RESULTS AND DISCUSSION

The synthetic conditions, the crystalline phases, and the morphologies of different particle size- and shape-controlled monoclinic ErOOH and cubic Er_2O_3 materials are summerized in Table 1. These ErOOH and Er_2O_3 micro/nanomaterials were synthesized from the hydro-solvothermal reaction of erbium nitrates in one-phase water/ethanol/decanoic acid mixture at 120−180 °C for 24 h. In this synthesis, erbium nitrate, decanoic acid (DA), and water/ethanol were used as precursor, capping agent, and solvent, respectively. After the hydro-solvothermal synthesis, the products were

capped by DA molecules and precipitated in the bottom of the vessel. The final products can be redispersible in nonpolar organic solvents due to their hydrophobic surface. Note that the hydro-solvothermal reaction mechanism for the erbium compound formation in this one-phase (water/ethanol) system in the present work is essentially different from the nucleophile one of the erbium oxide formation in the two-phase (water−toluene) system as mentioned above.[28] A variety of well-defined morphologies of monoclinic ErOOH and Er_2O_3 micro/nanostructures can also be obtained at the different reaction temperature stages and various reaction conditions in the synthesis process. The advantage of the current synthetic procedure is the use of erbium nitrate as an inexpensive starting material and water−ethanol as environmentally benign solvents, as compared to the traditional synthetic pathway, in general, using organic solvent, erbium alkoxides, or organometallics as expensive compounds.

Generally, surfactant-capped particles are hydrophobic, and ethanol is usually used to precipitate the particles out of the nonpolar solvents. It should be noted that, for the given synthetic conditions (Er^{3+} concentration, DA/Er, C_2H_5OH/H_2O, reaction temperature), the nucleation and growth has occurred in the bulk solution. The particles were spontaneously precipitated when they reached a critical size owing to their hydrophobic surface and the polar water/ethanol solution. The precipitated particles were confined and essentially isolated from the bulk solution. Further crystal growth of these particles could occur due to the minimization of facet surface energy, however, only in the intraparticles. The size and shape of the final particle products were essentially not disturbed by the growth process, as discussed in our recent paper.[10]

The procedure for the synthesis of these materials is illustrated in Scheme 1. At early stages, erbium nitrate was hydrolyzed in the water/ethanol solution in the presence of decanoic acid surfactant to generate erbium hydroxide nucleus. Resulting DA-capped $Er(OH)_3$ nucleus then dehydrated and grew into ErOOH particles in the synthesis solution at relatively low temperatures (120−140 °C). These ErOOH particles were converted into Er_2O_3 ones in the hydro-solvothermal treatment at higher temperatures (160−180 °C).[27] The results in this study (see below) indicate that phase and morphology of ErOOH and Er_2O_3 micro/nanoparticles can be easily controlled by only changing the reaction temperature. A series of temperature-dependent experiments were performed to understand the formation of erbium compound micro/nanostructures. The synthesis reactions were carried out at different temperatures (120, 140, 160, and 180 °C) for 24 h of each stage of temperature using the same starting chemical composition mixture (*e.g.*, $[Er^{3+}]$ = 7.63 mM, DA/Er = 5:1, 30 mL of C_2H_5OH, and 10 mL of H_2O).

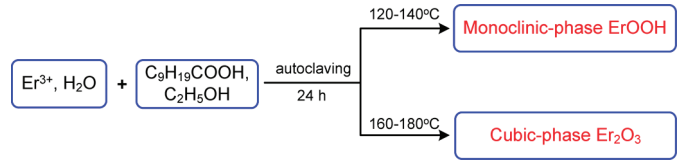

Scheme 1. General synthetic procedure for controlled size, shape, and phase of erbium compound micro- and nanostructures.

The X-ray diffraction (XRD) patterns of the erbium compound samples obtained at different reaction temperatures, while keeping other synthetic conditions unchanged, are shown in Figure 1. For the samples prepared at low temperatures (120 and 140 °C), the XRD patterns (Figure 1a,b) exhibit representative reflections for the monoclinic phase (ErOOH, $P2_1/m$, JCPDS 76-0700),[32,33] and no other phase was observed, indicating that only pure monoclinic-phase ErOOH products were formed. As the reaction temperature increases to 160 and 180 °C, the XRD patterns (Figure 1c,d) of these samples reveal the cubic-phase Er_2O_3 crystals with lattice constants of a = 4.753 Å, b = 5.720 Å, and c = 4.968 Å ($Fm3m$, JCPDS 08-0050).[28] This indicates that the cubic Er_2O_3 phase instead of the monoclinic ErOOH one was formed at higher temperatures. The broadening and intense diffraction peaks indicate small particle size and well-crystallized products. The average particle sizes of all the erbium compound samples from the (222) peak using the Scherrer equation were ~25 nm, implying that the ErOOH and Er_2O_3 microstructures were constructed from the aggregation of the small nanoparticles.

The TGA−DTA curves (Figure 2) were recorded for DA-capped ErOOH quasi-microspheres (sample 1). The TGA curve shows that the total weight loss of the DA-capped ErOOH microsphere sample is ~36%, which is attributed to the combustion/elimination of decanoic acid and the dehydration of the conversion of ErOOH into Er_2O_3. An intense exothermic peak at 313 °C along

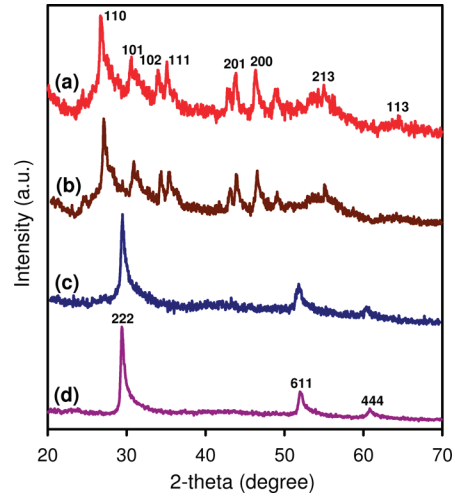

Figure 1. XRD patterns of the erbium compound micro/nanostructures synthesized at different reaction temperatures: (a) monoclinic ErOOH, 120 °C; (b) monoclinic ErOOH, 140 °C; (c) cubic Er_2O_3, 160 °C; and (d) cubic Er_2O_3, 180 °C.

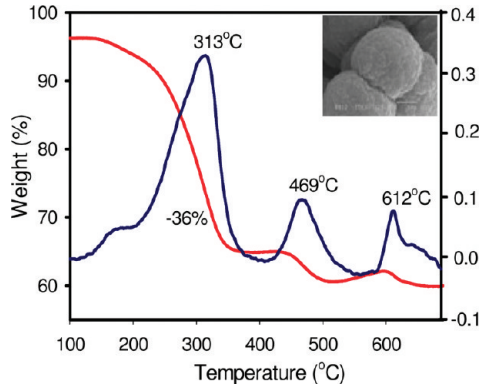

Figure 2. TGA−DTA curves of DA-capped ErOOH quasi-microspheres (sample 1 in Table 1).

with a weak peak at 469 °C in the DTA profile is attributed to the combustion and elimination of decanoic acids, respectively. The total weight loss of this stage (up to 500 °C) determined from the TGA curve is ~32.5%. In addition, the weight loss due to the dehydration of ErOOH into Er_2O_3 is ~3.5%, corresponding to a weak exothermic DTA peak at higher temperature (~612 °C). This experimental value (~3.5%) is consistent with the theoretical value of ~4%, as the dehydration of 2ErOOH to $Er_2O_3 + H_2O$. Therefore, it can be concluded that monoclinic ErOOH is a metastable phase, whereas the cubic Er_2O_3 phase is formed stable at high temperature.

The morphologies of the final products synthesized at different reaction temperatures in the range of 120−180 °C were also examined by the SEM technique (Figures 3 and 4). When the synthesis reaction was performed at 120 °C, as shown in Figure 3a,b, the ErOOH product is composed of quasi-microspherical aggregates with an average diameter of approximately 3 μm and a coalescence of small particles on their surface. This indicates that the quasi-spherical aggregates consist of small particles, in agreement with the XRD result. When the reaction temperature was increased to 140 °C, ErOOH microspherical aggregates were still observed and microspheres were however deformed, while the diameter of individual microspheres is essentially intact and their surface is rather rough (Figure 3c,d). The surface morphology change should be due to the classical ion-mediated growth process in intraparticles because of the difference in chemical potential on the particle surface (Ostwald ripening) at 140 °C.[34]

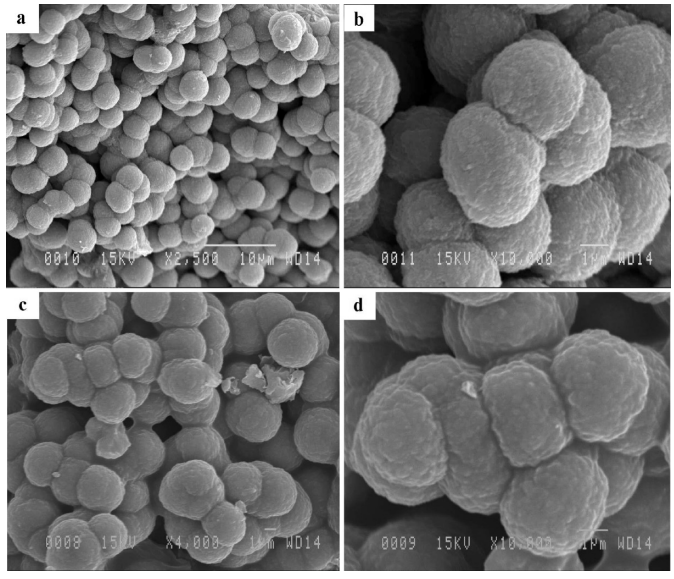

Figure 3. Different magnification SEM images of the ErOOH samples synthesized with the DA/Er ratio of 5/1 at different reaction temperatures: (a,b) quasi-microspheres, at 120 °C; (c,d) attached microspheres, at 140 °C.

At higher reaction temperature (>160 °C), the product was converted from monoclinic ErOOH into cubic Er_2O_3 phase, as seen in Figure 1. It is important to note that the Er_2O_3 microsphere morphology was significantly changed. Most wrinkle-surfaced microspheres with an average diameter of ~3 μm were observed (Figure 4a). These wrinkle-surfaced microspheres are attached together to form chainlike microsphere aggregates. From the enlarged SEM image (Figure 4b), the structure of the spherical architecture was built from several dozen nanoplates with smooth surfaces. The nanoplates with a thickness of ~200 nm and a length of ~1.0 μm were connected to each other to form spherical hierarchical structures. The closer inspection of the SEM images reveals that the size of these microspheres seems to be unchanged. However, the formation of the wrinkle-surfaced microspheres may be due to the etching of Er_2O_3 microsphere surfaces in the presence of decanoic acid at this temperature.[35]

Eventually, when the synthesis reaction was performed at 180 °C, the microspheres were surrounded by the nanorods gathered together into larger Er_2O_3 microflowers (Figure 4c,d). Each microflower consists of a number of nanorods, which is adhibited with each other to construct the assembled microflowers with an average diameter of each aggregate of approximately 3 μm. A careful observation of the enlarged SEM images in several parts of this sample clearly demonstrated that each petal of the microflowers is of rodlike morphology. A number of nanorods were found to be highly oriented, vertically aligned with high density, and extended outward from the center of each microflower. Each individual nanorod has an average diameter of ~0.1 μm and a length of ~0.7 μm. It may be established that a fractional oriented assembly of the nanorods at high reaction temperatures arises in situations far from thermodynamic equilibrium where high driving force leads to the generation of the ordered microflower assembly.[36]

Furthermore, with a fixed DA/Er molar ratio of 20:1 instead of DA/Er = 5:1, a series of experiments were also carried out at different temperatures from 120 to 160 °C; a similar trend (from the pure monoclinic ErOOH phase to the pure cubic Er_2O_3) was also observed by the XRD spectra (data not shown). Moreover, the

products exhibit magnificent morphologies, as seen in Figure 5. At 120 °C, the main ErOOH products were bundles of nanowires with a diameter of about 100 nm and a length in the range of 0.4 μm (Figure 5a). At 140 °C, the abundance of nearly monodisperse ErOOH straw nanosheaves with rough surface and the nanowire aggregates were formed (Figure 5b). The TEM image inset of Figure 5c clearly shows individual so-called ErOOH straw nanosheaves which are strongly twisted in the middle part, leading to the formation of the fanned dual fantails. These straw nanosheaves with their extended dual fantails are closely bonded to each other in the middle part and have a length in the range of 700 nm, a fantail diameter of about 150 nm, and a middle diameter of about 70 nm. When the reaction temperature was increased to 160 °C, the morphologies of ErOOH nanoarchitectures were almost broom bundles with a broom diameter of about 150 nm and a length in the range of 350−400 nm (Figure 5d). The SAED pattern (inset of Figure 5c) of the straw nanosheaves clearly shows bright diffraction rings indicating that the nanowires as building units of the hierarchical nanobundle assemblies are polycrystalline rather than single crystalline. These small thin nanowires have a higher chemical potential owing to a larger length-to-diameter ratio and thus are easier to coalesce, leading to the nanobundles with lower surface energy.[37] In addition, the formation of the nanobundles for this DA/Er ratio (20:1) in the bulk solution could be illustrated by the lateral aggregation mechanism due to relatively short alkyl chain of capping decanoic acid (C_{10}), in agreement with those reported by our group.[38,39]

The decanoic acid (DA) concentration in the bulk solution was also found to play a crucial role in the size- and shape-controlled synthesis of erbium oxide nanocrystals. To investigate this parameter, a series of experiments were carried out at 180 °C with different DA concentrations, from 0.038 to 0.228 M in the bulk solution (*e.g.*, the DA/Er molar ratio increases from 5:1 to 30:1), while the other parameters were kept the same ($[Er^{3+}]$ = 7.63 mM, 30 mL of C_2H_5OH, 10 mL of H_2O). Interestingly, the products exhibit size/shape-dependent DA concentration change. At the same reaction temperature (180 °C), increasing the DA concentration from 0.038 to 0.228 M, the particle size decreases from ~3 μm to ~3 nm (Figures 4c,d and 6). At relatively low DA concentrations, 0.038 M (*e.g.*, DA/Er = 5:1) and 0.076 M (*e.g.*, DA/Er = 10:1), Er_2O_3 microflowers with an average diameter of ~3 μm were found (see Figures 4c,d and 6a). However, at higher DA concentrations, only nanoparticles with different shapes were formed. When the DA/Er ratio was increased to 15:1, 18 nm sized dog-bond-like nanocrystals companied with some nanocubes were found (Figure 6b). Only uniform 18 nm sized nanospheres were formed, while the DA/Er ratio reached 20:1 (Figure 6c). Furthermore, the nano-

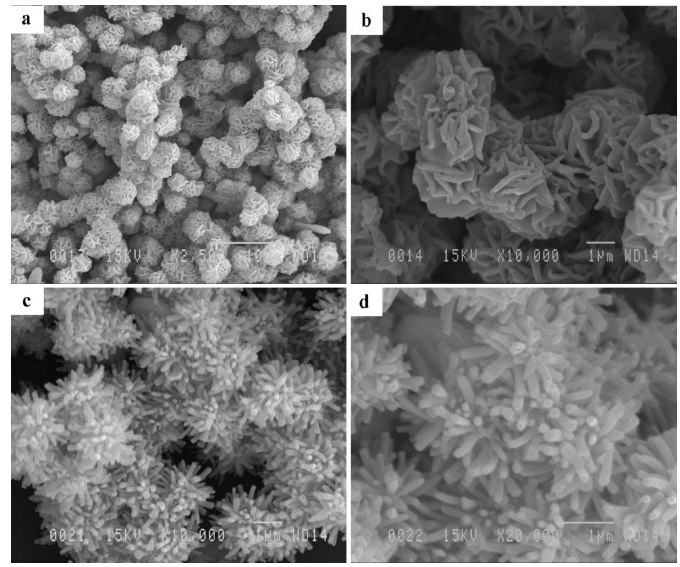

Figure 4. Different magnification SEM images of the Er_2O_3 samples synthesized with the DA/Er ratio of 5/1 at different reaction temperatures: (a,b) wrinkle-surfaced microspheres, at 160 °C; (c,d) microflowers, at 180 °C.

dots with an average diameter of 3 nm were produced with DA/Er = 30:1 (Figure 6d).

The SAED pattern (inset of Figure 6c) of the Er_2O_3 nanospheres taken from a single sphere is indexed respectively to the strong concentric rings from the (222), (400), (440), and (622) planes of a single cubic Er_2O_3 structure. The XRD patterns exhibit a pure cubic-phase Er_2O_3 structure for the both samples of Er_2O_3 nanospheres and nanodots (Figure 7, samples 10 and 11 in Table 1). Compared to the diffraction peaks for the erbium compound microstructures, the XRD peaks for the Er_2O_3 nanospheres/nanodots are much broader,

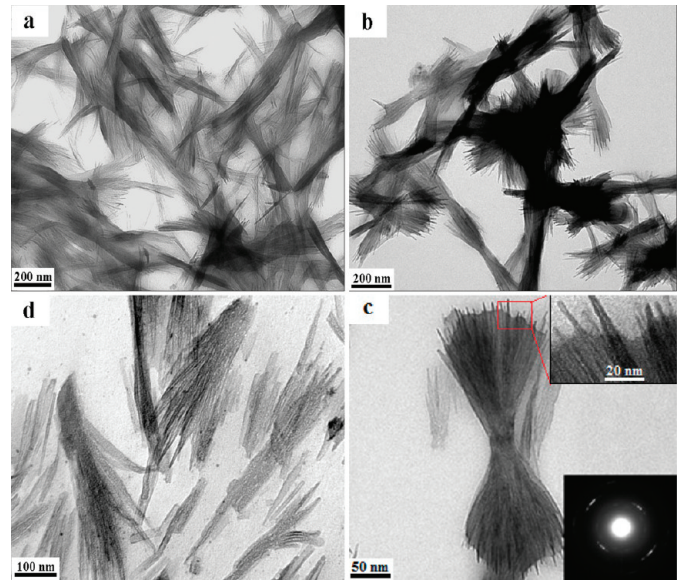

Figure 5. TEM images of the erbium compound nanostructures synthesized with the DA/Er molar ratio of 20:1 at different reaction temperatures: (a) ErOOH wire nanobundles, at 120 °C; (b,c) ErOOH straw nanosheaves, at 140 °C, inset SAED; (d) Er_2O_3 broom nanobundles, at 160 °C.

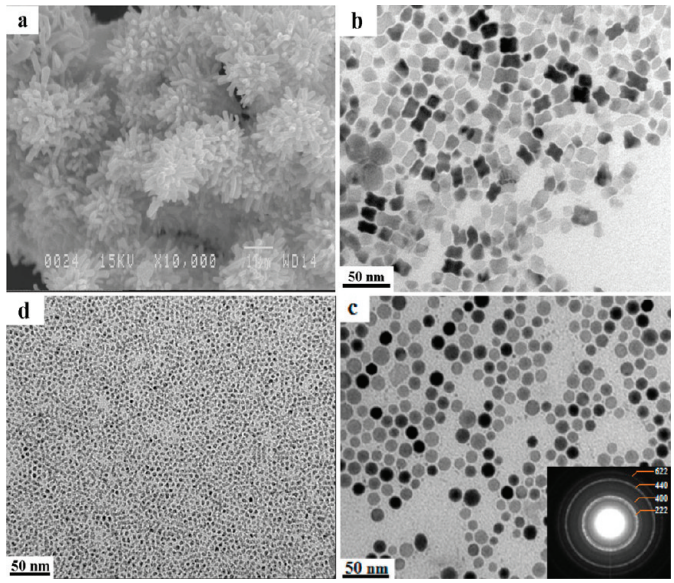

Figure 6. SEM/TEM images of the Er_2O_3 micro- and nanotructures synthesized at 180 C, in ethanol−water medium (ethanol/water ratio of 30:10 mL) with different DA/Er molar ratios: (a) 3 μm microflowers, DA/Er = 10:1; (b) 18 nm dog-bond-like nanocrystals, DA/Er = 15:1; (c) 18 nm nanospheres, DA/Er = 20:1, inset SAED; (d) 3 nm nanodots, DA/Er = 30:1.

implying a smaller particle size. According to the Scherrer equation, the mean particle sizes of nanospheres and nanodots are estimated from the (222) peak to be about 16.0 and 4.5 nm, respectively, which are consistent with the TEM results.

The reason for the size/shape-dependent DA concentration evolution should be due to the covering degree of capping agent on the particle surface. The above results suggest that the surfactant (decanoic acid) serves not only as a stabilizer to prevent the aggregation of the products but also as a strong shape controller assisting to the formation of erbium compound crystals during the crystal growth process. It is consistent with our previous results on the size-controlled synthesis of $SmVO_4$ nanospheres using oleylamine as capping agent.[40,41]

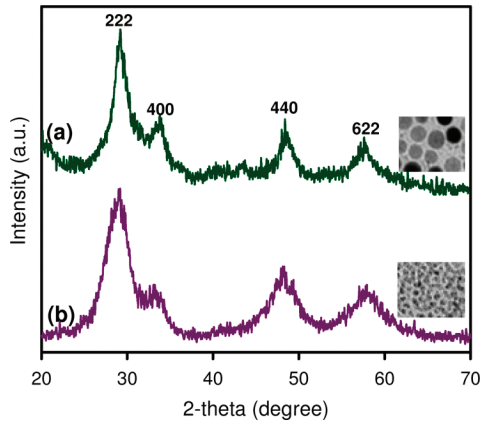

Figure 7. XRD patterns of the Er_2O_3 samples: (a) nanospheres (sample 10) and (b) nanodots (sample 11 in Table 1).

In order to study the effect of water content, nature of precursor, and precursor monomer concentration in bulk solution on size and shape of the final products, a series of experiments with different synthetic conditions were also carried out at 180 °C for 24 h with the Er/DA molar ratio of 20:1: (i) without water; (ii) with water; (iii) different erbium precursors, $Er(NO_3)_3$ and $Er(OH)_3$; (iv) different $Er(OH)_3$ concentrations, [$Er(OH)_3$] = 7.63, 76.25, 152.50 mM, respectively (see Table 1). $Er(OH)_3$ gel was prepared by adjusting the pH to 12 in the aqueous erbium nitrate solution using 10% NaOH (see Experimental Section). The TEM/SEM images of these products are shown in Figure 8. The case of sample 12 was synthesized under the same synthetic conditions (*e.g.*, $Er(NO_3)_3$ = 7.63 mM) of sample 10 in Table 1 (Figure 6c), except that anhydrous ethanol (40 mL) was used as a reaction solvent instead of ethanol/water (30:10 mL) mixture. Uniform self-assembled Er_2O_3 nanocores with ~3 nm diameter were obtained (sample 12 in Table 1 and Figure 8a). This indicates a decrease in particle size of erbium oxide nanospheres from 18 to 3 nm when only anhydrous ethanol was used as reaction medium. Futhermore, with the same ethanol/water ratio of 30:10 (mL), when $Er(OH)_3$ precursor was substituted by $Er(NO_3)_3$, 4 nm sized Er_2O_3 nanodots (sample 13 in Table 1 and Figure 8b) were yielded instead of ~18 nm sized nanospheres (Figure 6c). The effect of erbium precursors, $Er(NO_3)_3$ and $Er(OH)_3$, on particle size in this case could be mainly due to its influence on the pH of the reaction solution (*e.g.*, pH ~6 and 9.0, respectively).[27]

The $Er(OH)_3$ precursor concentration can also play a significant role in the morphological evolution of the products. As the $Er(OH)_3$ monomer concentration increased from 7.63 to 76.25 mM, the particle size and shape changed from 4 nm sized Er_2O_3 nanodots to 80 nm × 150 nm sized Er_2O_3 nanowires (samples 13 and 14 in Table 1 and Figure 8b,c). When the precursor concentration increased to 152.50 mM, the products are mainly rods with ~0.25 μm in width and ~1 μm in length. These microrods were organized the aligned parallel to form a large bundle (sample 14 and Figure 8d). This suggests that the growth of anisotropic structures occurred at a relatively high reactant concentration due to a relatively high chemical potential environment in the bulk solution.[42] Figure 9 shows the XRD patterns of the as-synthesized samples of nanocores and microrods (samples 12 and 15 in Table 1). Both samples starting from $Er(OH)_3$ precursors exhibit a pure cubic-phase Er_2O_3 structure, suggesting that the dehydration of erbium hydroxides to oxides occurs during hydrosolvothermal treatment at this temperature (180 °C). On the basis of the above experimental results, a schematic diagram of the growth process for the formation of monoclinic ErOOH and cubic Er_2O_3 micro/nanostructures in size and shape as a function of synthesis

temperature and surfactant/precursor molar ratio is summarized in Scheme 2.

The X-ray photoelectron spectra (XPS) of the ErOOH quasi-microspheres (sample 1) and Er_2O_3 microflowers (sample 4) were measured to examine the chemical surface composition and oxidation state of erbium in erbium compound structures. The survey XPS spectra reveal that these samples (not shown data) contain Er 4d, O 1s, and C 1s, while no impurites were detected. The high-resolution Er 4d XPS spectra are presented in Figure 10A. Both samples exhibit the Er 4d states characterizing Er^{3+} in ErOOH and Er_2O_3 structures.[43] However, the Er 4d XPS spectrum of the ErOOH sample is composed of five component peaks at binding energies of 168.8, 171.0, 173.0, 184.0, and 196.6 eV, while the Er 4d XPS spectrum of the Er_2O_3 sample consists of only four corresponding components and the absence of peak at 171.0 eV. Furthermore, the difference of the O 1s XPS spectra of the ErOOH and Er_2O_3 samples was also observed (Figure 10B). The ErOOH sample is composed of two oxygen components, whereas the Er_2O_3 sample exhibits only one oxygen component. For the ErOOH sample, the weak XPS peak at 529.4 eV is assigned to the HO−Er groups, and the intense second one at 531.8 eV is attributed to the O−Er groups. The Er_2O_3 sample exhibits only one O 1s XPS peak at 531.8 eV related to O−Er bonds. This also indicates a high OH concentration on the particle surface of the ErOOH sample.

Figure 11A shows the C 1s XPS spectrum of the DA-capped ErOOH sample (sample 1). This spectrum consists of three peaks at 285.8, 286.0, and 288.8 eV which correspond to C−C, C═C, and C−C═O of decanoic acid molecules, respectively. The C 1s XPS spectrum (data not shown) of the DA-capped Er_2O_3 sample also exhibits a similar result of sample 1. One photograph of the transparent white- and rose-colored toluene solution containing the as-synthesized ErOOH nanospheres and Er_2O_3 nanoflowers, respectively, is shown in the inset of Figure 11A. A clear solution indicates that ErOOH and Er_2O_3 particles were highly dispersed in toluene. These clearly suggest that the erbium compound micro/nanomaterials were capped by the carboxyl groups of decanoic acid molecules, and as a consequence, the exposed hydrophobic alkyl groups were well-immersed in toluene.[44] To further confirm this result, the FTIR spectra were also recorded for the two DA-capped ErOOH and Er_2O_3 samples (samples 1 and 4 in Table 1) and are shown in Figure 11B. Both samples exhibit an absorption band at 670 cm^{-1}, which is characteristic of the Er−O stretching mode. The O−H stretching mode for the ErOOH sample was also observed at 3700 cm^{-1}, which is a typical FTIR band of structural OH groups for erbium oxyhydroxide.[33] The FTIR bands at 2864−2944 cm^{-1} attributed to the C−H stretching mode of alkyl chains of decanoic acid molecules were observed for the two samples.[37] Two FTIR bands were observed at 1466 and 1548 cm^{-1}, which are attributed

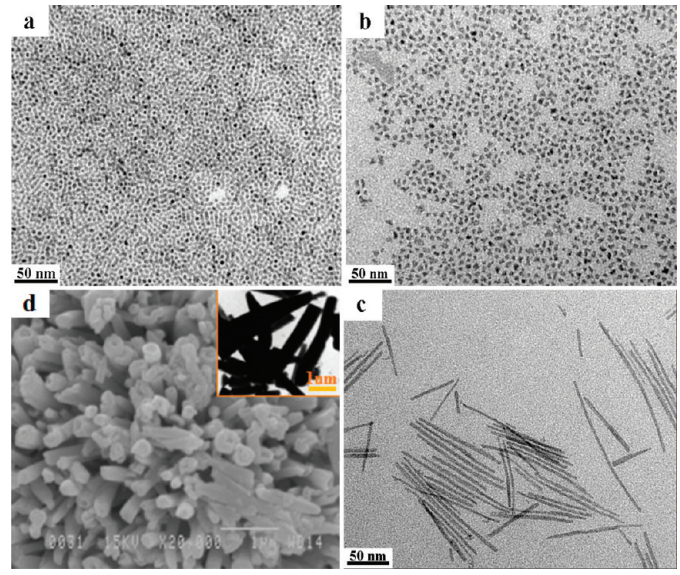

Figure 8. TEM/SEM images of the Er_2O_3 samples synthesized with DA/Er = 20:1 at different reaction conditions: (a) ~3 nm nanocores, $[Er(NO_3)_3]$ = 7.63 mM without water; (b) ~4 nm nanodots, $[Er(OH)_3]$ = 7.63 mM, ethanol/water = 30:10 (mL); (c) 80 nm × 150 nm nanowires, $[Er(OH)_3]$ = 76.25 mM, ethanol/water = 30:10 (mL); (d) 250 nm × 1000 nm microrods, $[Er(OH)_3]$ = 152.50 mM, ethanol/water = 30:10 (mL).

to the symmetric and asymmetric stretching vibrations of the carboxylate groups of decanoic acid, respectively.[37] A large band around 3500 cm^{-1} corresponds to the O−H stretching frequency of surface hydroxide groups, which were observed in the ErOOH sample, in good agreement with the above XPS results. These data further confirm that the carboxylic groups of decanoic acid molecules capped on the particle surface.

The optical properties of micro/nanostructures of ErOOH and Er_2O_3 in toluene were characterized by UV/vis absorption and photoluminescence (PL) spectroscopy (Figure 12). The UV/vis spectra (Figure 12A) of 3 μm ErOOH quasi-microspheres (sample 1) and 18 nm Er_2O_3 nanospheres (sample 10 in Table 1) exhibit different peak shapes and the maximum excitonic peak shifted from 280 to 289 nm, illustrating the difference from the ErOOH and Er_2O_3 crystals.[33] It is also noteworthy that the color of the final products changed from

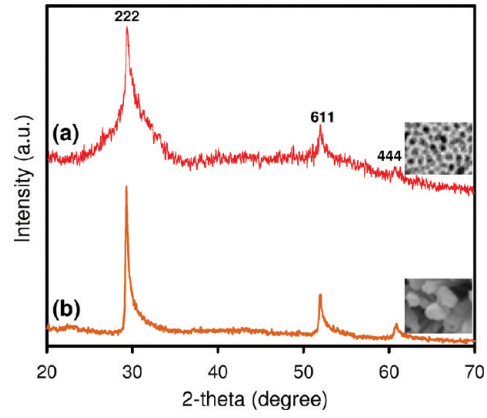

Figure 9. XRD patterns of the Er_2O_3 samples: (a) nanocores (sample 12) and (b) microrods (sample 15 in Table 1).

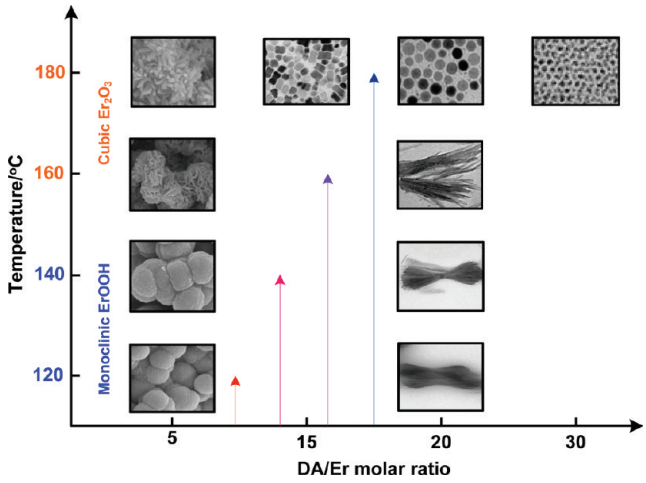

Scheme 2. ErOOH and Er_2O_3 micro- and nanostructures with different sizes, shapes, and phases obtained as a function of reaction temperature and decanoic acid/erbium molar ratio.

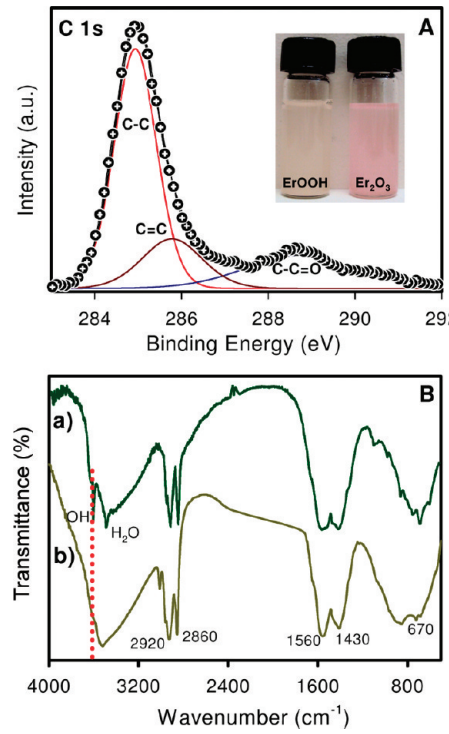

Figure 11. (A) C 1s XPS spectrum of DA-capped ErOOH quasi-microspheres; (inset) one photo of transparent white- and rose-colored toluene solution containing the as-synthesized ErOOH nanospheres and Er_2O_3 nanoflowers, respectively. (B) FTIR spectra of (a) DA-capped ErOOH quasi-microspheres (sample 1) and (b) DA-capped Er_2O_3 microflowers (sample 4 in Table 1).

white to light rose with the change from monoclinic ErOOH to cubic Er_2O_3 phase (*e.g.*, increasing the reaction temperature from 120 to 180 °C, inset of Figure 12A). The upconversion luminescence properties of various samples with different particle size, ErOOH wire nanobundles (sample 5) and ErOOH quasi-microspheres (sample 1), compared with those of Er_2O_3 nanospheres (sample 10) and Er_2O_3 microflowers (sample 4) under 218 nm excitation are presented in Figure 12B,C. The colloidal solutions of the ErOOH and Er_2O_3 samples both show the different excitonic peak shapes but the same spectral peak positions corresponding to the following 4f−4f transitions: $^2H_{9/2} \rightarrow {}^4I_{15/2}$ (~424 nm), $^4F_{3/2} \rightarrow {}^4I_{15/2}$ (~448 nm), $^4F_{7/2} \rightarrow {}^4I_{15/2}$ (~485 nm), $^4S_{3/2} \rightarrow {}^4I_{15/2}$ (~560 nm).[33,45] In a comparison of the peak intensity, this indicates that erbium compound nanospheres/nanobundles clearly show much stronger luminescence than erbium compound microspheres. This is due to the decrease of particle size in both cases: ErOOH and Er_2O_3 particles. These results can indicate that the decrease of particle size leads to the increase of the number of active atoms located on the exposed particle surfaces.[25,46] As a result, the luminescence intensity is strongly related to quantum confinement effect and the change of the excited energy between valence band and conduction band of these materials.[47]

These results contribute to the understanding of the size and shape control of erbium compound particles from micro- to nanostructure. This synthetic approach allows generation of a variety of shape-, size-, and phase-controlled erbium compound materials using erbium nitrate salts as a starting material and

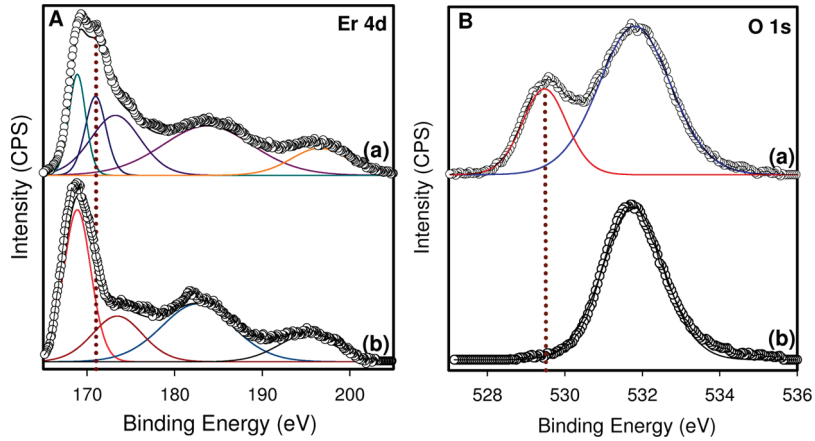

Figure 10. High-resolution XPS spectra of (A) Er 4d and (B) O 1s for (a) 3 μm ErOOH quasi-microspheres (sample 1) and (b) 3 μm Er_2O_3 microflowers (sample 4 in Table 1).

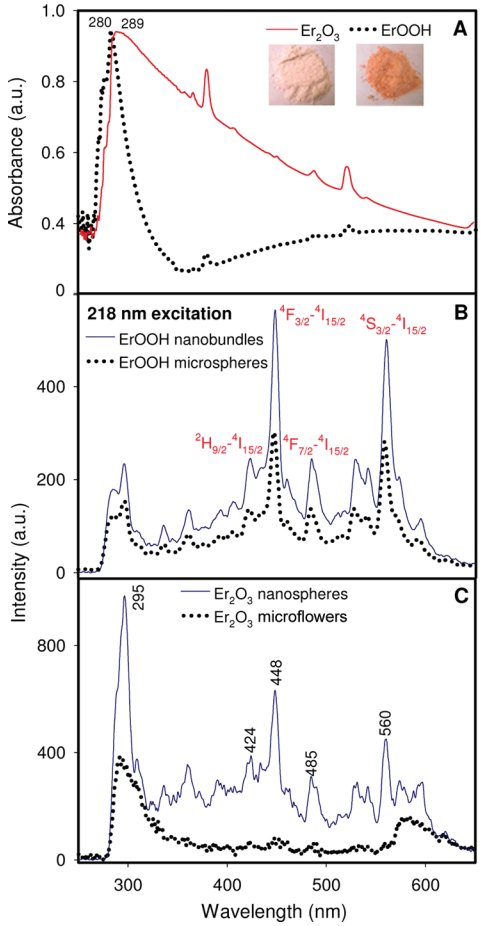

Figure 12. (A) UV/vis absorption spectra of 3 μm ErOOH quasi-microspheres (sample 1) and 18 nm Er_2O_3 nanospheres (sample 10), (inset) pictures show color change of the final products at different synthesis temperatures. Photoluminescence (PL) spectra of (B) 100 nm × 400 nm ErOOH wire nanobundles (sample 5) and 3 μm ErOOH quasi-microspheres (sample 1); (C) 18 nm Er_2O_3 nanospheres (sample 10) and 3 μm Er_2O_3 microflowers (sample 4 in Table 1).

water/ethanol as an environmental solvent. This work is studied systematically in this type of nanomaterial. We believe that these materials with manifold morphologies will be useful for the further investigation of their optical telecommunications and sensing applications.

CONCLUSION

In conclusion, the micro- and nanostructures of monoclinic ErOOH and cubic Er_2O_3 particles with different size and a variety of shapes have been synthesized by the hydro-solvothermal reaction using erbium nitrate and decanoic acid as precursor and capping agent in the water−ethanol medium at temperature of 120−180 °C for 24 h. After the synthesis reaction, the nanoparticle products were capped by the carboxylic groups of decanoic acid molecules and precipitated in the bottom of an autoclave cup due to their hydrophobic surface and the polar water−ethanol medium. This water/ethanol-based approach provides a simple, versatile, high-yield, and inexpensive pathway for the synthesis of a variety of erbium compound micro/nanoarchitectures. The monoclinic ErOOH phase can be obtained at 120−140 °C and the cubic Er_2O_3 phase at 160−180 °C.

The ErOOH and Er_2O_3 particles with different sizes from 3 nm to 3 μm and shapes including cores/dots to spheres, wrinkle-surfaced spheres, flowers, dog bonds, wires, rods, bundles, straw sheaves, and brooms can be manipulated simply by controlling the reaction parameters. With increasing the decanoic acid concentration from 0.038 to 0.190 M, the particle size of the product decreased from micro- to nanometer. Furthermore, when water/ethanol (10:30 mL) was replaced by anhydrous ethanol, the particle size significantly decreased from 18 nm (nanospheres) to 3 nm (nanocores). The nanorod products were also achieved with high precursor monomer concentrations, from 76.25 to 152.50 mM, due to the anisotropic growth. The upconversion luminescence results indicate that the luminescence properties depend not only on the crystalline phase but also on the particle size of products. The luminescence intensity increases with a decrease of particle size. It is expected that monoclinic ErOOH and cubic Er_2O_3 micro/nanostructures with manifold morphologies will lead to new opportunities for further practical applications in optical telecommunications and other fields.

EXPERIMENTAL SECTION

Chemicals: All chemicals were used as received without further purification. Erbium nitrate hexahydrate ($Er(NO_3)_3 \cdot 6H_2O$, 99.9%) and decanoic acid ($C_{10}H_{22}COOH$ or DA, technical grade, 70%) were purchased from Sigma-Aldrich. Anhydrous ethanol and sodium hydroxide were purchased from Reagent ACS.

Synthesis of ErOOH and Er_2O_3 Micro/Nanostructures: $Er(NO_3)_2 \cdot 6H_2O$ (0.30−6.10 mmol) was dissolved in 10 mL of distilled water to form a clear light rose-colored solution. A homogeneous ethanol solution (30 mL) containing decanoic acid (1.52−9.15 mmol) was added into the above solution under magnetic stirring for 10 min. The obtained mixture was transferred into a 70 mL autoclave with a Teflon linear at 120−180 °C for 24 h. The DA-capped products were collected in the bottom of the Teflon cup and can redisperse in nonpolar organic solvents (*e.g.*, toluene or hexane). Erbium compound micro/nanoparticles with different phases, sizes, and shapes were obtained following similar procedures by varying the reaction temperature, the surfactant/precursor molar ratio, the concentration and nature of precursor, and water content in the synthesis solution. In the case of using $Er(OH)_3$ as precursor instead of erbium nitrate salt, $Er(OH)_3$ gel was prepared by adjusting the pH value in the aqueous erbium nitrate solution using 10% NaOH. Typically, $Er(NO_3)_2 \cdot 6H_2O$ (0.135−2.700 g) was dissolved in 50 mL of distilled water to form a clear light rose-colored solution. The pH was then adjusted with a 10% NaOH aqueous solution to 12. After being stirred for about 30 min, the rose-colored $Er(OH)_3$ precipitate gel was filtered and washed several times with deionized water to remove ionic remnants. The obtained $Er(OH)_3$ gel was dispersed in 10 mL of distilled water. The reaction solutions (40 mL) with different precursor concentrations (7.63, 76.25, 152.50 mM) were prepared by mixing aqueous $Er(OH)_3$ gel solution (10 mL) and

anhydrous ethanol solution (30 mL) containing decanoic acid (6.09 mmol).

Characterization: The X-ray diffraction (XRD) patterns were recorded on a Bruker SMART APEXII X-ray diffractometer, using Cu Kα radiation (λ = 1.5418 Å). Scanning electron microscope (SEM) images of products were obtained from a JEOL 6360 instrument working at 3 kV. Transmission electron microscope (TEM) images and selected area electron diffraction (SAED) of the samples were obtained on a JEOL JEM 1230 operated at 120 kV. Samples were prepared by placing a drop of a dilute toluene dispersion of crystals onto a 200 mesh carbon-coated copper grid and immediately evaporated at ambient temperature. XPS measurements were carried out in an ion-pumped chamber (evacuated to 10^{-9} Torr) of a photoelectron spectrometer (Kratos Axis-Ultra) equipped with a focused X-ray source (Al Kα, *hv* = 1486.6 eV). The binding energy of the samples was calibrated by setting the C 1 s peak to 285 eV. The peaks were deconvoluted by means of a standard CasaXPS software (v.2.3.13; product of CasaXPS Software Ltd., USA) to resolve the separate constituents after background subtraction. The thermal analyses of DA-capped ErOOH quasi-microspheres (~5 mg) were carried out at a heating rate of 10 °C/min, under an air flux up to 700 °C using a Perkin-Elmer TGA thermogravimetric analyzer. Fourier transform infrared absorption spectra (FTIR) were measured with a FTS 45 infrared spectrophotometer with the KBr pellet technique. The UV−visible spectra of the micro/nanostructures were recorded for the powder sample on a Cary 300 Bio UV−visible spectrophotometer, and pure toluene was used as a blank. Room temperature photoluminescence spectra were measured on an optical spectrum analyzer (ANDO AQ6317, Japan).

Acknowledgment. This work was supported by the Natural Sciences and Engineering Research Council of Canada (NSERC) through a strategic grant.

REFERENCES AND NOTES

1. Min, Y.; Akbulut, M.; Kristiansen, K.; Golan, Y.; Israelachvili, J. The Role of Interparticle and External Forces in Nanoparticle Assembly. *Nat. Mater.* **2008**, *7*, 527–538.
2. Wang, D.; Lieber, C. M. Inorganic Materials: Nanocrystals Branch Out. *Nat. Mater.* **2003**, *2*, 355–356.
3. El-Sayed, M. A. Some Interesting Properties of Metals Confined in Time and Nanometer Space of Different Shapes. *Acc. Chem. Res.* **2001**, *34*, 257–264.
4. Gao, J.; Gu, H.; Xu, B. Multifunctional Magnetic Nanoparticles: Design, Synthesis, and Biomedical Applications. *Acc. Chem. Res.* **2009**, *42*, 1097–1107.
5. Xiong, Y.; Wiley, B. J.; Xia, Y. Nanocrystals with Unconventional Shapes-A Class of Promising Catalysts. *Angew. Chem., Int. Ed.* **2007**, *46*, 7157–7159.
6. Zhuang, J.; Shaller, A. D.; Lynch, J.; Wu, H.; Chen, O.; Li, A. D. Q.; Cao, Y. C. Cylindrical Superparticles from Semiconductor Nanorods. *J. Am. Chem. Soc.* **2009**, *131*, 6084–6085.
7. Shang, N.; Papakonstantinou, P.; Wang, P.; Zakharov, A.; Palnitkar, U.; Lin, I.; Chu, M.; Stamboulis, A. Self-Assembled Growth, Microstructure, and Field-Emission High-Performance of Ultrathin Diamond Nanorods. *ACS Nano* **2009**, *3*, 1032–1038.
8. Choi, S. H.; Kim, E. G.; Hyeon, T. One-Pot Synthesis of Copper-Indium Sulfide Nanocrystal Heterostructures with Acorn, Bottle, and Larva Shapes. *J. Am. Chem. Soc.* **2006**, *128*, 2520–2521.
9. Soumare, Y.; Garcia, C.; Maurer, T.; Chaboussant, G.; Ott, F.; Fievet, F.; Piquemal, J. Y.; Viau, G. Kinetically Controlled Synthesis of Cobalt Nanorods with High Magnetic Coercivity. *Adv. Funct. Mater.* **2009**, *19*, 1–7.
10. Cao, T. D.; Nguyen, T. D.; Kleitz, F.; Do, T. O. Shape-Controlled Synthesis of Highly Crystalline Titania Nanocrystals. *ACS Nano* **2009**, *3*, 3737–3743.
11. Wang, X.; Li, Y. Monodisperse Nanocrystals: General Synthesis, Assembly, and Their Applications. *Chem. Commun.* **2007**, 2901–2910.
12. Lou, X. W.; Archer, L. A.; Yang, Z. Hollow Micro-/Nanostructures: Synthesis and Applications. *Adv. Mater.* **2008**, *20*, 3987–4019.
13. Ratke, L.; Voorhees, P. W. *Growth and Coarsening: Ostwald Ripening in Material Processing*; Springer: Berlin, 2002; pp 117−118.
14. Tang, J.; Alivisatos, A. P. Crystal Splitting in the Growth of Bi_2S_3. *Nano Lett.* **2006**, *6*, 2701–2706.
15. Zhao, N. N.; Pan, D. C.; Nie, W.; Ji, X. L. Two-Phase Approach for the Synthesis of Shape-Controlled Colloidal Zirconia Nanocrystals. *J. Am. Chem. Soc.* **2006**, *128*, 10118–10124.
16. Philippe, C.; *et al. Erbium-Doped Fiber Amplifiers (Optics and Photonics)*; Academic Press: New York, 1999.
17. Solehmainen, K.; Kapulainen, M.; Heimala, O.; Polamo, M. Erbium-Doped Waveguides Fabricated with Atomic Layer Deposition Method. *IEEE Photon Technol. Lett.* **2004**, *16*, 194–196.
18. Michael, C. P.; Yuen, H. B.; Sabnis, V. A.; Johnson, T. J.; Sewell, R.; Smith, R.; Jamora, A.; Clark, A.; Semans, S.; Atanackovic, P. B.; *et al.* Growth, Processing, and Optical Properties of Epitaxial Er_2O_3 on Silicon. *Opt. Express* **2008**, *16*, 19649–19666.
19. Sun, R. G.; Wang, Y. Z.; Zheng, Q. B.; Zhang, H. J.; Epstein, A. J. 1.54 μm Infrared Photoluminescence and Electroluminescence from an Erbium Organic Compound. *J. Appl. Phys.* **2000**, *87*, 7589.
20. Shuto, K.; Hattori, K.; Kitagawa, T.; Ohmori, Y.; Horiguchi, M. Erbium-Doped Phosphosilicate Glass Waveguide Amplifier Fabricated by PECVD. *Electron. Lett.* **1993**, *29*, 139.
21. Feng, W.; Sun, L.; Zhang, Y.; Yan, C. Solid-to-Hollow Single-Particle Manipulation of a Self-Assembled Luminescent $NaYF_4$:Yb, Er Nanocrystal Monolayer by Electron-Beam Lithography. *Small* **2009**, *5*, 2057–2060.
22. Heer, S.; Kompe, K.; Gudel, H.; Haase, M. Highly Efficient Multicolour Upconversion Emission in Transparent Colloids of Lanthanide-Doped $NaYF_4$ Nanocrystals. *Adv. Mater.* **2004**, *16*, 2102–2105.
23. Yang, J.; Li, C.; Quan, Z.; Zhang, C.; Yang, P.; Li, Y.; Yu, C.; Lin, J. Self-Assembled 3D Flowerlike Lu_2O_3 and Lu_2O_3:Ln^{3+} (Ln = Eu, Tb, Dy, Pr, Sm, Er, Ho, Tm) Microarchitectures: Ethylene Glycol-Mediated Hydrothermal Synthesis and Luminescent Properties. *J. Phys. Chem. C* **2008**, *112*, 12777–12785.
24. Yin, S.; Akita, S.; Shinozaki, M.; Li, R.; Sato, T. Synthesis and Morphological Control of Rare Earth Oxide Nanoparticles by Solvothermal Reaction. *J. Mater. Sci.* **2008**, *43*, 2234–2239.
25. Wang, G.; Peng, Q.; Li, Y. Upconversion Luminescence of Monodisperse CaF_2:Yb^{3+}/Er^{3+} Nanocrystals. *J. Am. Chem. Soc.* **2009**, *131*, 14200–14201.
26. Han, K.; Zhang, Y.; Fang, Z.; Cheng, T.; Gao, M. A Simple Route to Preparation and Characterization of Er_2O_3 Microspheres. *Chem. Lett.* **2007**, *36*, 1124–1125.
27. Wang, X.; Li, Y. Rare-Earth-Compound Nanowires, Nanotubes, and Fullerene-like Nanoparticles: Synthesis, Characterization, and Properties. *Chem.—Eur. J.* **2003**, *9*, 5627–5635.
28. Nguyen, T. D.; Do, T. O. General Two-Phase Routes to Synthesize Colloidal Metal Oxide Nanocrystals: Simple Synthesis and Ordered Self-Assembly Structures. *J. Phys. Chem. C* **2009**, *113*, 11204–11214.
29. Depner, S. W.; Kort, K. R.; Jaye, C.; Fischer, D. A.; Banerjee, S. Nonhydrolytic Synthesis and Electronic Structure of Ligand-Capped $CeO_{2-\delta}$ and CeOCl Nanocrystals. *J. Phys. Chem. C* **2009**, *113*, 14126–14134.
30. Park, J.; An, K.; Hwang, Y.; Park, J. G.; Noh, H. J.; Kim, J. Y.; Park, J. H.; Hwang, N. M.; Hyeon, T. Ultra-Large-Scale Syntheses of Monodisperse Nanocrystals. *Nat. Mater.* **2004**, *3*, 891–895.
31. Oaki, Y.; Imai, H. Chelation-Mediated Aqueous Synthesis of Metal Oxyhydroxide and Oxide Nanostructures: Combination of Ligand-Controlled Oxidation and Ligand-Cooperative Morphogenesis. *Chem.—Eur. J.* **2007**, *13*, 8564–8571.

32. Christensen, A. N. N.; Quezel, S. The Magnetic Structure of The Monoclinic Modification of ErOOH. *Solid State Commun.* **1972**, *10*, 765–767.
33. Assaaoudi, H.; Fang, Z.; Butler, I. S.; Kozinski, J. A. Synthesis of Erbium Hydroxide Microflowers and Nanostructures in Subcritical Water. *Nanotechnology* **2008**, *19*, 185606.
34. Jun, Y. W.; Choi, J. S.; Cheon, J. Shape Control of Semiconductor and Metal Oxide Nanocrystals through Nonhydrolytic Colloidal Routes. *Angew. Chem., Int. Ed.* **2006**, *45*, 3414–3439.
35. An, K.; Kwon, S. G.; Park, M.; Na, H. B.; Baik, S. I.; Yu, J. H.; Kim, D.; Son, J. S.; Kim, Y. W.; Song, I. C.; *et al.* Synthesis of Uniform Hollow Oxide Nanoparticles through Nanoscale Acid Etching. *Nano Lett.* **2008**, *8*, 4252–4258.
36. Ban, T.; Nakatani, T.; Uehara, Y.; Ohya, Y. Microstructure of Six-Pointed Starlike Anatase Aggregates. *Cryst. Growth Des.* **2008**, *8*, 935–940.
37. Zhao, D.; Yang, Q.; Han, Z.; Sun, F.; Tang, K.; Yu, F. Rare Earth Hydroxycarbonate Materials with Hierarchical Structures: Preparation and Characterization, and Catalytic Activity of Derived Oxides. *Solid State Sci.* **2008**, *10*, 1028–1036.
38. Nguyen, T. D.; Mrabet, D.; Do, T. O. Controlled Self-Assembly of Sm_2O_3 Nanoparticles into Nanorods: Simple and Large Scale Synthesis Using Bulk Sm_2O_3 Powders. *J. Phys. Chem. C* **2008**, *112*, 15226–15235.
39. Nguyen, T. D.; Do, T. O. Solvo-Hydrothermal Approach for the Shape-Selective Synthesis of Vanadium Oxide Nanocrystals and Their Characterization. *Langmuir* **2009**, *25*, 5322–5332.
40. Nguyen, T. D.; Cao, D. T.; Dinh, T. N.; Do, T. O. A Novel Approach for Monodisperse Samarium Orthovanadate Nanocrystals: Controlled Synthesis and Characterization. *J. Phys. Chem. C* **2009**, *113*, 18584–18595.
41. Nguyen, T. D.; Dinh, C. T.; Do, T. D. Monodisperse Samarium and Cerium Orthovanadate Nanocrystals and Metal Oxidation States on the Nanocrystal Surface. *Langmuir* **2009**, *25*, 11142–11148.
42. Peng, Z. A.; Peng, X. Nearly Monodisperse and Shape-Controlled CdSe Nanocrystals *via* Alternative Routes: Nucleation and Growth. *J. Am. Chem. Soc.* **2002**, *124*, 3343–3353.
43. Swami, G. T. K.; Stageberg, F. E.; Goldman, A. M. XPS Characterization of Erbium Sesquioxide and Erbium Hydroxide. *J. Vac. Sci. Technol., A* **1984**, *2*, 767–770.
44. Deng, Z.; Peng, B.; Chen, D.; Tang, F.; Muscat, A. J. A New Route to Self-Assembled Tin Dioxide Nanospheres: Fabrication and Characterization. *Langmuir* **2008**, *24*, 11089–11095.
45. Que, W.; Zhou, Y.; Lam, Y. L.; Pita, K.; Chan, Y. C.; Kam, C. H. Luminescence Properties from Erbium Oxide Nanocrystals Dispersed in Titania/Organically Modified Silane Composite Sol−Gel Thin Films. *Appl. Phys. A: Mater. Sci. Process.* **2001**, *73*, 209–213.
46. Devaraju, M. K.; Yin, S.; Sato, T. A Rapid Hydrothermal Synthesis of Rare Earth Oxide Activated $Y(OH)_3$ and Y_2O_3 Nanotubes. *Nanotechnology* **2009**, *20*, 305302.
47. Yin, S.; Shinozaki, M.; Sato, T. Synthesis and Characterization of Wire-like and Near-Spherical Eu_2O_3-Doped Y_2O_3 Phosphors by Solvothermal Reaction. *J. Lumin.* **2007**, *126*, 427–433.